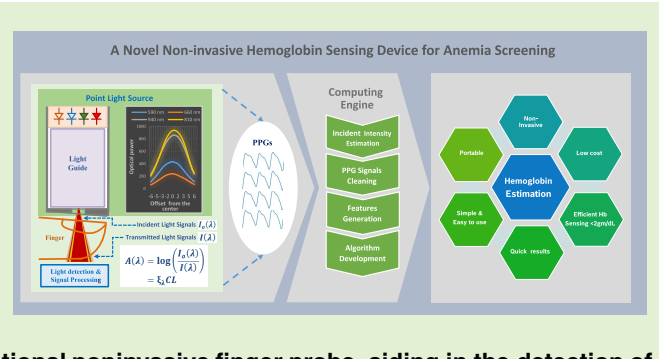


A Novel Noninvasive Hemoglobin Sensing Device for Anemia Screening

R. Dinesh Kumar[✉], S. Guruprasad, Krity Kansara[✉], K. N. Raghavendra Rao[✉], Murali Mohan, Manjunath Ramakrishna Reddy, Uday Haleangadi Prabhu, P. Prakash, Sushovan Chakraborty[✉], Sreetama Das[✉], and K. N. Madhusoodanan

Abstract—Anemia is a condition that affects more than a billion people globally, with the highest prevalence noticed among women and children. In large parts of the world anemia is detected by using invasive laboratory techniques that require blood draw by trained doctors, nurses or laboratory staff. A low cost and easy to use noninvasive device that can be used at the doorstep or bedside of a patient has the potential to create a significant impact in anemia screening. In this paper, we present the architecture and development of such a device. Using a specific arrangement of light emitting diodes and fiber optics, we have created a novel multiwavelength spectrophotometry sensing platform to detect anemia. A mechanical lever operated fiber optics based sensor eliminates the problems associated with conventional noninvasive finger probe, aiding in the detection of hemoglobin levels as low as 1.6 g/dL. This study also proposes a method wherein incident light intensity can be measured along with attenuated light intensity to support hemoglobin estimation. The device could detect the light signals as low as 0.001% of the incident light intensity. Performance of the proposed platform was validated in conjunction with an algorithm to estimate hemoglobin. The device was able to estimate hemoglobin with an RMSE of 1.47 ± 0.042 g/dL and a correlation of 0.79 ± 0.03 between the predicted and actual value of Hb.

Index Terms—Anemia, hemoglobin, noninvasive, photo plethysmography, point light source, spectrophotometry.



I. INTRODUCTION

ANEMIA is a condition in which hemoglobin concentration in blood is lower than a predefined normal. Millions of people are suffering from anemia especially pregnant women and children. Traditional anemia detection methods rely on invasive methods like blood draw. These conventional blood draw procedures are painful, have probability of infection, require consumables, a biohazard disposal system and trained technicians. These reasons also make these methods less accessible and expensive for the rural population. An affordable, easy to use, noninvasive anemia screening device, accessible to the less-privileged, is still commercially unavailable.

Manuscript received February 14, 2021; revised March 23, 2021; accepted March 23, 2021. Date of publication April 5, 2021; date of current version June 30, 2021. The associate editor coordinating the review of this article and approving it for publication was Prof. Tarikul Islam. (*Corresponding author: R. Dinesh Kumar.*)

R. Dinesh Kumar is with the Department of Instrumentation, Cochin University of Science and Technology (CUSAT), Kochi 682022, India, and also with Robert Bosch (RBEI), Bengaluru 560095, India (e-mail: dineshkumar.rayaroth@in.bosch.com).

S. Guruprasad, Krity Kansara, K. N. Raghavendra Rao, Murali Mohan, Manjunath Ramakrishna Reddy, Uday Haleangadi Prabhu, P. Prakash, Sushovan Chakraborty, and Sreetama Das are with Robert Bosch (RBEI), Bengaluru 560095, India.

K. N. Madhusoodanan is with the Department of Instrumentation, Cochin University of Science and Technology (CUSAT), Kochi 682022, India.

Digital Object Identifier 10.1109/JSEN.2021.3070971

Mostly, the studies revolving around noninvasive hemoglobin photo-plethysmography based sensors to estimate/monitor blood hemoglobin noninvasively, other studies propose three-wavelength light emitting diode (LED) [4]–[8], and five-LED based multiwavelength sensors [9]. Yi *et al.* [10], on the other hand proposed methods based on dynamic spectrum and spectrum extraction algorithms to develop an instrument design with eight laser diodes. However, these device architectures are usually followed by hemoglobin quantification being implemented separately on a laptop/personal computer using a prediction algorithm. C. Pinto *et al.* have recently combined a five LED based finger probe with an arduino based embedded system solution [11] as a step towards a standalone device architecture. Similarly, Liu *et al.* [12] have developed a portable prototype employing eight LEDs for noninvasive estimation of hemoglobin, but the performance of these prototypes have been tested on a small datasets and across a narrow range of hemoglobin values.

Lasers have also been experimented with for similar applications, making use of their narrow spectral width and better transmittance [10], of light through the finger tissue. Nitzan *et al.* [13], used lasers and trifurcated fiber optic bundles as optical couplers to combine lights from multiple sources and create a point light source. However, laser setups are often heavy and accompanied with special driving circuits to maintain a constant temperature since laser

TABLE I
SUMMARY OF COMMERCIALLY AVAILABLE HEMOGLOBIN
ESTIMATION DEVICES

Name of the device	Invasive / Noninvasive	Technology used	Time to result (Secs) *	Supported range of Hemoglobin (g/dL)	Price (USD) *
True Hb Hemometer	Invasive	Reflectance Photometry	< 60	4-20 (<5% tolerance)	~ 70 - 100
TouChb (Biosense)	Noninvasive	Reflectance Photometry	60	No range specified	~ 700
OrSense 200 NBM	Noninvasive	Occlusion spectroscopy	~ 60	7-17	~ 1500 - 2000
Masimo Pronto Pulse Co-Oximeter	Noninvasive	Signal Extraction Technology	-	8 to 17	~ 2000
Hemospect	Noninvasive	Transcutaneous reflection spectroscopy	20-30	8 to 17	-

*Disclaimer: Taken from public domain.

wavelengths are temperature dependent [14], and need to be biased above a threshold current level. These reasons make the conventional laser-based systems relatively expensive and complex deeming them less suitable to be implemented as standalone, cost-effective, simple portable devices. Recent researches based on Optofluidic DFB lasers [15], and highly sensitive optical nano biosensors [16]–[18], show promise in spectrophotometry applications because of their compactness, lower threshold energy levels and low cost. Studies with small footprint sensing devices in the field of bio-sensing [19] using nanotechnology have also been reported. Graphene plasmonic sensor [18], [19] is a one such promising candidate for bio-sensing in the near infrared range. High sensitivity, compactness and tunability [18] are the main advantages of these nano structure based sensors. Although, such viable optofluidic DFB lasers or nano structure based biosensors are still not commercially available for noninvasive applications.

On the other hand, Wang *et al.* [20], presented HemaApp, a smartphone application that can monitor hemoglobin concentration using the Nexus-5 smartphone camera and other light sources. Although promising, HemaApp is not only yet robust to different hardware (different cameras, lenses, and filters) and architectures of mobile phones but also has high variability in signal quality especially for lower hemoglobin concentrations. Masimo's Pronto, Haemospect and OrSense NBM 200 are a few noninvasive anemia detection devices currently available commercially [21], [22], summarized in Table I. However, studies highlight their limitations in severely anemic scenarios along with large estimated limits of agreement [23]–[25].

In the present study, we attempted to address such limitations by improvising the device architecture and introducing a few techniques that can enhance the performance of a noninvasive hemoglobin estimation device. We aspired to realize a stand-alone, easy-to-carry battery-operated device architecture capable of capturing PPG signals robustly and processing them to estimate hemoglobin values of an individual at point-of-care, especially in remote locations, which could address anemia management especially for the rural population.

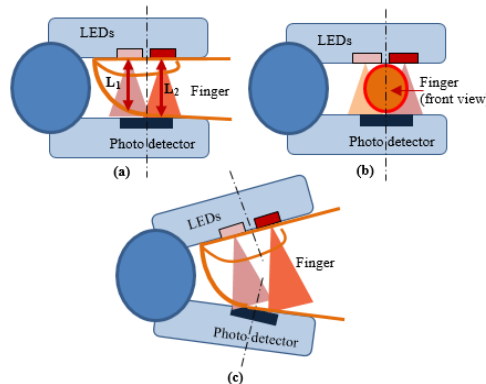


Fig. 1. Issues with conventional transmission mode *jaw-type* probes employing multiple light sources (two LEDs shown in figure) with respect to finger geometry and finger sizes. (a) Unequal path lengths for multiple light sources; (b) Optical bypassing for small fingers/wide light source assemblies; and (c) Lack of alignment between light source and photodetector for thick fingers.

A. Jaw-Type Finger Probes

The conventional transmission mode *jaw-type* finger-clip PPG acquisition probe when used with multiple light sources, gives rise to a few issues owing to its design. Fig. 1 provides a geometrical illustration of a few such issues. In laboratory-based blood hemoglobin estimations, measurements are done on the light absorbed by a cuvette filled with blood sample. In this case, the thickness (or width) of the cuvette remains constant. On the other hand, in *jaw-type* finger probe assemblies [9], [21], the amount of light absorbed by a finger is measured. In this case, the thickness of the finger may not always be uniform. Also, in case of multiple light sources, the path length of absorption for each light source may vary (Fig. 1(a)). In two wavelength pulse oximetry, optical path length is assumed as constant for both wavelengths [26]. If path length is different for multiple light sources as in Fig 1(a), light attenuation due to tissue absorption will be different for each wavelength which causes error in computation of hemoglobin concentration. If the light source assembly is too wide with respect to the finger, there are chances of optical bypassing [27], [28], wherein some amount of light may reach the photo detector directly instead of passing through the finger (Fig. 1(b)). Optical bypassing weakens the PPG signals and leads to error in measurements, especially in case of thin fingers. Optical interference due to ambient light (sunlight or bright external light sources) may also add to such errors [28], [29]. If the size of the finger is too large, the light sources and the photo detector may not line up properly. For very thick fingers, light penetrating through the finger may not reach the detector (Fig. 1(c)). Additionally, in scenarios where the finger probe is connected via cables, signal-to-noise ratio is susceptible to the noise picked by the cable and the strength of signal picked by the photodetector.

Another crucial step to a better estimation of hemoglobin using spectrophotometry is the accurate measurement of intensity of incident light. This is because degradation of intensity of the light source over time affects the measurements. Takamura *et al.* [30], reports the use of a phantom with a known light absorbing characteristic to measure the

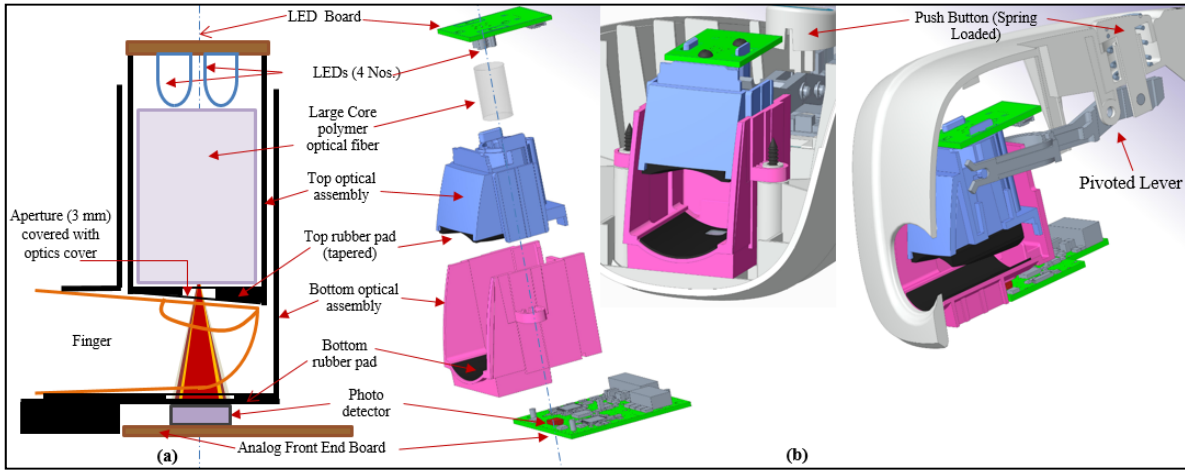


Fig. 2. Diagram illustrating the arrangement of the point-source sensor assembly. The problems of multiple path lengths, optical bypassing and misalignment are eliminated by ensuring that the point light source, the finger slot and the photodetector are always in a straight line for all finger sizes.

incident intensity. Limitation of this technique is the requisite and precise positioning of the phantom whenever incident light intensity is to be measured. Here, we propose two novel techniques to measure the incident light intensity without the need of a phantom.

In this study, we propose a point-light-source architecture to eliminate the problems associated with multi-wavelength jaw-type finger probes and the method to calculate incident intensity such that the measurements are not affected by the degradation of light source intensity over time. The following sections of this article are arranged as follows. We begin with describing the components of the proposed device architecture assembly, followed by description of the experimental setups and their results.

II. MATERIALS AND METHODS

A. Device Architecture

The proposed device architecture consists of the following components: (i) single-point light source; (ii) finger slot; (iii) photodetector and analog front end (AFE) board; (iv) Single Board Computer (SBC) (Fig. 2(a)).

The problems of multiple path lengths, optical bypassing and misalignment are eliminated by ensuring that the point light source, the finger slot and the photodetector are always in a straight line for all finger sizes. The components of the architecture are described in detail below.

1) Single-Point Light Source (Top Assembly): The single-point light source assembly comprises of: (i) four through hole LEDs mounted in close proximity to each other on a small printed circuit board (PCB) and (ii) a fiber optic guide that collects the light from all LEDs and emits it through an aperture, which in turn falls onto the finger. This arrangement ensures a uniform path length for absorption. High intensity, narrow emission angle (~ 30 degree) LEDs and large core fiber optic guide (10mm diameter) made of PolyMethyl MethAcrylate (PMMA) were chosen. PMMA was chosen because of its low transmission losses at wavelengths used for the light sources. A wide acceptance angle (80°) was chosen for the fiber optics guide to ensure maximum

coupling between the light from the LED and the optical fiber. Transmission of light through the optical fiber was done via total internal reflection. The length of the optical fiber was chosen such that light from all four LEDs has a uniform light intensity distribution. Both end faces of the optical fiber were polished to minimize scattering and reflection losses. Fig. 2 shows the arrangement of the single-point light source assembly. This assembly is attached with a spring-loaded push button with a pivoted lever. When the push button is pressed, the lever lifts the top optics assembly upwards thereby causing a linear up/down movement of the top assembly in line with the photodetector.

2) Finger Slot (Bottom Assembly): The finger is inserted in the finger slot during measurement. A flexible tapered silicon rubber pad is provided above the finger slot to accommodate for the curved geometry of the finger. The finger is allowed to rest on a thin finger pad which has an opening, aligned in line with the single-point light source. The opening in the finger pad can be (optionally) covered with an optics cover made of PMMA. The top and bottom assemblies form a closed sensing mechanism which prevents the ambient light from being picked by the photodetector.

3) Analog Front End Board: Analog front end (AFE) board consists of: (i) a photodetector, (ii) two AFE4490 modules and (iii) a computing unit. The photodetector is mounted on AFE board to capture the amount of light coming out of the finger. It is a surface mounted silicon pin photodiode with a spectral response range of 400nm to 1100nm and active area of $2.5\text{mm} \times 2.5\text{mm}$. It is used to convert the optical signal to an analogous electrical signal. Four Photoplethysmograms (PPGs) corresponding to the four LED wavelengths are generated by this photodetector for one measurement. The absence of the traditional cable connecting the photodetector and AFE avoids the signal loss due to transmission. Fig. 3 shows the AFE board block diagram and top level architecture of the device.

The purpose of the AFE board is to digitize the four PPG signals and store the data in the AFE registers. Two standard two-channel AFE modules (AFE4490 from Texas Instruments)

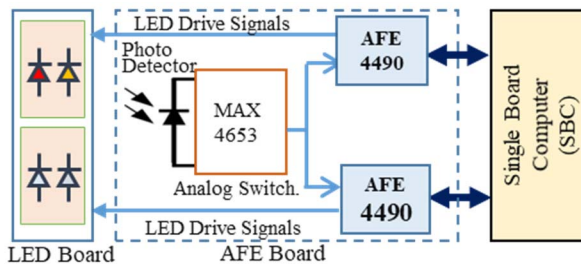


Fig. 3. AFE board block diagram and Top level architecture of the device.

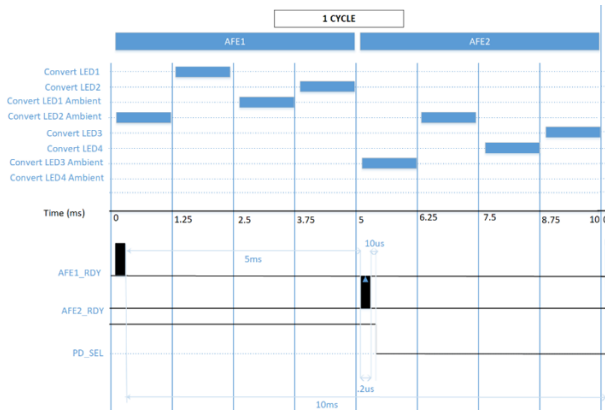


Fig. 4. Computing unit timing diagram of one complete cycle (10ms).

were used in the study. AFE4490 has an in-built circuitry for two-channel LED transmitter and a photodetector receiver. The optical receiver circuitry consists of a transimpedance amplifier for converting the photodiode current to an amplified voltage, signal filtering, and ambient noise cancellation and analog to digital conversion. Two such modules drove the four LEDs and processing the photodetector current. An analog switch synchronized the single photodetector between both AFE4490 modules. The leakage current of the switch is 0.1 nA; the input-referred noise current of the AFE module is 50 pA_{RMS} and the dark current of the photodetector is negligible at zero bias voltage. The three of these collectively decide the minimum intensity of light signal that can be detected by the system.

A computing unit (single board computer) generates the timing and control signals to coordinate the operation of the two AFE4490 modules and to switch the photodetector between them to drive the four LEDs sequentially at an operating frequency of 100 Hz (Fig. 4). It configures AFE's registers for activation of all LEDs, enables data sampling and digitization. Once an AFE is configured, it generates an AFE_RDY interrupt for the processor to read the AFE register data. AFE_RDY interrupt is used to toggle the photo detector select (PD_SEL) signal used for switching the detector between AFE1 and AFE2.

4) Single Board Computer (SBC): The SBC used in this study was designed using i.MX6ULL series ARM cortex A7 processor with operating frequency of 528 MHz, 512 MB RAM (DDR3L) and 8 GB flash memory (EMMC). Device is powered by a single Li-Ion cell. Battery management circuit was provided for charging the Li-Ion cell. Internet connectivity

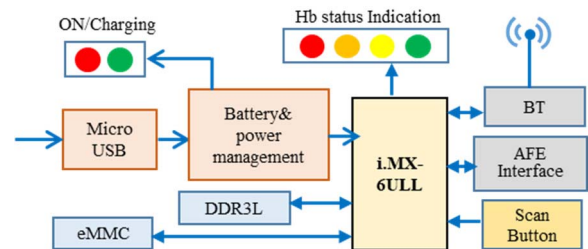


Fig. 5. Block diagram of SBC unit.

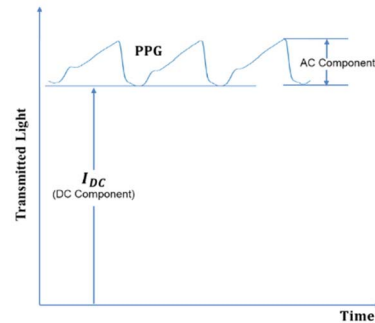


Fig. 6. Components of a PPG signal.

was enabled using an inbuilt Wi-Fi module (IEEE802.11b/g/n) so that the device has the capability to send the data from the device to the cloud (IoT). The block diagram of the SBC is shown in Fig. 5.

The purpose of the SBC is to receive the four digitized PPG signals from AFE board and processes them. The steps of processing include filtering of signals, extraction of features, and estimation of blood hemoglobin value using an algorithm housed on the SBC and generating an output file with results.

B. Principle of Operation

The principle of operation of the proposed device architecture is based on the Beer-Lambert's law, which states that the amount of light absorbed by an analyte depends on the concentration (C), absorbing path length (L) and absorptivity constant (ξ_λ) of the absorbent at a wavelength (λ). This law is mathematically expressed in (1)

$$I = I_o e^{-\xi_\lambda \cdot C \cdot L} \quad (1)$$

where, I is the transmitted intensity of the light and I_o is the incident intensity. A PPG signal consists of a DC component and a pulsatile AC component (Fig. 6). The DC component (I_{DC}) is due to the absorption of skin, tissue, venous blood etc. The AC component is generated from the pulsatile arterial blood flow. AC component is taken to be proportional to the blood hemoglobin concentration as in equation (1).

Light intensity at the photodetector(mWatt)

$$= P K L 10^{-OD} \quad (2)$$

Ouput voltage

$$= (P K L 10^{-OD}) RG \quad (3)$$

where, P is the LED light intensity, K is coupling factor for the light coupled from LED to light guide, L is the transmission

loss of light guide and OD is the optical density of the finger at the LED wavelength, R is the responsivity of the photodetector (mA/mW) and G is the gain of the transimpedance amplifier of AFE module.

Total blood hemoglobin comprises of four subcomponents - oxyhemoglobin (HbO_2), reduced hemoglobin (RHb), carboxyhemoglobin (HbCo) and methemoglobin (HbMet). The wavelengths of the four LEDs used in the proposed device architecture were chosen based on the absorption spectra of these hemoglobin subcomponents and the optical density of the skin. Two wavelengths from the visible spectrum: 590 nm and 660 nm, intended to maximize absorption of HbCo and HbO_2 ; and two wavelengths from near infrared region: 810 nm and 940 nm, intended to maximize absorption of HbMet and RHb respectively, were selected [31].

Transmission loss due to absorption and scattering of light for PMMA fiber was 0.8 dB/metre for the wavelength range of 400-1000 nm. The loss corresponding to the length of the optical fiber guide chosen for this study was calculated to be 0.016 dB (<0.4%) and hence neglected during calculations.

The optical density (OD) of the human finger is >3 for visible and near infrared (NIR) wavelengths [32], which implies that >99.9% of incident light will be absorbed by the finger and only ~0.1% will reach the photodetector for sensing. Hence, LED light intensity along with LED spectral bandwidth and light emission angle were critical in influencing the quality of PPGs acquired from the device. The intensity of 590 nm LED was kept relatively high because of high OD value for this wavelength [32]. The spectral bandwidth for LEDs with wavelengths 590 nm and 660 nm was chosen to be 20 nm owing to steeper slopes of absorption spectrum of Hb components whereas the spectral bandwidth for LEDs with wavelengths 810 nm and 940 nm was chosen to be 40 nm since the absorption curves are relatively flat in these near-infrared regions [33].

Absorbance (A) at a wavelength λ was defined to represent the attenuated amount of light picked by the photodetector. In accordance with the Beer Lambert's law, this Absorbance value is proportional to the concentration of the component in the blood. Hence:

$$A(\lambda) = \log(I_o(\lambda)/I(\lambda)) = \xi_\lambda CL \quad (4)$$

Absorbance $AT(\lambda_1)$ corresponds to total Hb at λ_1 is given in (5)

$$AT(\lambda_1) = \log\left(\frac{I_o(\lambda_1)}{I(\lambda_1)}\right) = \sum_{n=1}^4 (\xi_n(\lambda_1) C_n L_n) \quad (5)$$

Four absorbance values corresponding to the four wavelengths of light were generated. Due to the advantage of a uniform path length of absorption for all four wavelengths, we could assume the variable L (path length) constant. Now, solving for the value of the variable C (concentration), we could estimate the sum of Hb subcomponents.

The PPG signals, once collected, are pre-processed to remove motion artefacts and other signal noises. A set of features are generated using the incident and attenuated light intensities. Incident intensities are measured and updated every time the device is switched on (explained in detail in

TABLE II
DIFFERENT COMBINATIONS OF LEDs AND COUPLING OPTICS

Combination1	Optical fiber + wide band emission SMD LEDs
Combination2	CPC + wide band emission SMD LEDs
Combination3	Tapered guide + wide band emission SMD LEDs
Combination4	Optical fiber + narrow band emission Though hole LEDs
Combination5	CPC + narrow band emission Though hole LEDs
Combination6	Tapered guide + narrow band emission Though hole LEDs
Combination7	Multiwavelength LED

the next section). Four attenuated intensity values and five ratio of ratios are calculated from the pulsatile components of four PPG waveforms corresponding to light from the four LEDs (590 nm, 660 nm, 810 nm and 940 nm). A total of eleven features are generated: four attenuation values; five ratio of ratios; age and pregnancy status. The details of feature generation and signal processing is explained in detail in the [34].

C. Experimental Setup

1) *Single-Point Light Source*: We experimented with three different sets of LEDs and three different light coupling methods in order to derive at the most optimum combination to form the single-point light source. The types of LEDs evaluated for this study were: (i) multiwavelength single LED; (ii) Surface Mount Device (SMD) LED with a wide emission pattern; (iii) through hole LED with narrow emission pattern. SMD LEDs were considered because they have flat surfaces and through hole LEDs were considered because they have a sharp emission pattern. Multiwavelength single LED provides an advantage of compactness relative to four individual LEDs.

The types of optical coupling methods evaluated were: (i) large core polymer optical fiber (10 mm diameter) from Edmund optics; (ii) Compound Parabolic Concentrator (CPC) from Edmund optics (input diameter: 9 mm, output diameter: 2.5 mm); (iii) tapered light guide. Optical guides were selected based on their spectral transmission range and size (diameter/aperture). The fiber and tapered Light Guide used total internal reflection to transmit the light. CPC on the other hand, collected and concentrated the light. Seven Combinations of these were formed, as listed under Table II. The characteristics of the LEDs and the optical guides are tabulated in Table III a and b respectively.

But, usually, SMD LEDs with flat surface have wide emission patterns whereas through hole LEDs with sharp emission patterns do not have flat emitting surfaces to aid in coupling. For the combination of four SMD LEDs and large core optical fiber with wide band emission (Combination1), the optical fiber was butt coupled to the LED surface because it was flat in shape. The length of the optical fiber was tuned to have a uniform light intensity profile. On the other hand, for the combination of though hole LEDs with narrow emission pattern and large core optical fiber (Combination4), the LED surface was not flat and hence butt coupling was not possible. However, the light emission angle of LED was lesser than the acceptance angle of the fiber, hence, the coupling was proper.

TABLE III
(A) CHARACTERISTICS OF LEDs FOR DIFFERENT GROUPS, (B) CHARACTERISTICS OF COUPLING OPTIC DEVICES

Group-1 (5.3 mm,5pin TO-CAN 18) Viewing Angle 110°		Group-2 (SMD 3.5mm X 2.7mm X 1.8mm) Viewing Angle Approx.110°		Group-3 (3 mm Through hole type) with Viewing Angle Approx. 34°	
Wavelength λ (nm)	Optical Power	Wavelength λ (nm)	Optical Power	Wavelength λ (nm)	Optical Power
Multi wavelength 569/660/ 805/940	569	0.08 mW at 20mA	Dual wavelength 660/940	940	2.6 cd at 20mA
	660	2.9 mW at 20mA		660	1.5 cd at 20mA
	805	3.5 mW at 20mA		810	22 mW at 50mA
	940	2.5 mW at 20mA		590	18 mW at 50mA

(b)					
Optical fiber		CPC		Tapered light guide	
Attenuation	0.8 dB/m	Input Diameter	10.77 mm	Input Aperture	2.5 x 2.5 mm
Diameter	10 mm	Output Diameter	5 mm	Output Aperture	7.5 x 7.5 mm
Minimum Bend Radius	8 X Diameter	Length	15.04 mm	Length	50.0 mm
Spectral Transmission Range	400-1000 nm	Spectral Transmission Range	350 nm – 2500 nm	Spectral Transmission Range	350 nm – 2500 nm
Acceptance Angle	80°	Acceptance Angle	45°		

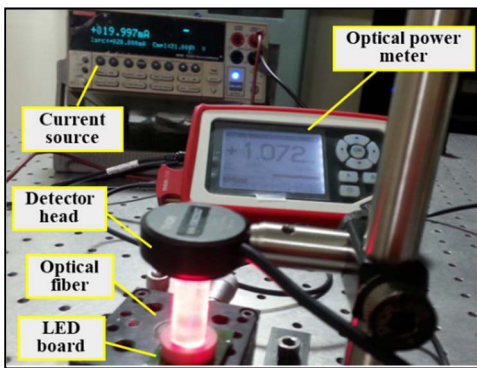


Fig. 7. Picture of the test set up used to measure the intensity distribution of the four LEDs for the seven combinations of LEDs and optical guide assemblies.

The seven combinations of the LED and optical guide assemblies were carried out to: (i) plot and assess the intensity distribution profile of the LEDs as detected by the photodetector; (ii) find out the amount of loss incurred in transmission and coupling; and (iii) assess the ease of mechanical integration. Intensity distribution of each of the four wavelengths was taken by driving one LED at a time.

Fig. 7 shows a picture of the experiment set up. LEDs were driven by constant current sources. Driving current for each LED was different. Optical coupling setup was aligned on the top of LED assemblies. A wide area photodetector head was positioned on the top of the coupling device. The sensing area of the photodetector was restricted to a small active area by using a mask with an aperture of 0.5 mm diameter. A small (0.5 mm diameter, 5 mm length) plastic clad silica optical fiber was attached to the aperture. The position of the photodetector was kept fixed and the LED-light coupling assembly was moved in fixed intervals (0.5 mm) in one direction, so that photodetector could scan the intensity of light coming out of the optical coupling setup.

The intensity distribution profiles of the four LEDs were plotted for the seven combinations. Power losses incurred while coupling the light from LED to the optical guide (Coupling losses) and during the transmission of light through

the optical guide (transmission losses) were observed in terms of the ratio of light coming out from the combination to the light emitted by the respective LED. The ease of mechanical integration was observed based on the shape and mechanical robustness of the optical guide. Combination4 was also tested for sensitivity, repeatability and accuracy of coupling by measuring the intensity distribution and peak offset in multiple trials.

2) Incident Intensity: The incident intensity of the device is usually measured by recording the intensity of light falling on the photodetector in the absence of the finger. Since this incident intensity cannot be directly measured with normal current and gain settings, we propose a method which involves the determination of two multiplication factors: current multiplication factor (CM) and a Gain multiplication factor (GM). To ensure that the electrical output generated by the photodetector amplifier is not saturated while measuring the incident intensity in the absence of the finger, a reduced current and gain settings can be configured. Hence, a separate configuration file of reduced LED current and reduced photodetector amplifier gain for all four wavelengths were used to estimate incident intensity. The actual incident intensity value was then calculated from this reduced intensity value by multiplying it with a current multiplication factor (CM) and a gain multiplication factor (GM). The CM and GM for a device could be calculated and stored in the memory of the device during production. These factors can be determined by two different methods as explained below. Device will measure the reduced intensity whenever it is turned ON and estimate the actual incident intensity using multiplication factors which is already stored in the device (Eq. 6).

$$\text{Actual Incident intensity} = \text{Reduced intensity} \times \text{CM} \times \text{GM} \quad (6)$$

Method-1: This method uses predetermined multiplication factors by taking the ratio of normal setting value and reduced setting value. If, for the first LED, the normal LED current setting is I_{N1} , the normal photodetector amplifier gain setting is G_{N1} , the reduced LED current setting is I_{R1} and the reduced



Fig. 8. Picture of the ND filter used in the study to calculate the incident intensity multiplication factors.

TABLE IV

STEPS FOR CALCULATING THE MULTIPLICATION FACTOR USING METHOD-2 EMPLOYING THE ND FILTER

Steps	LED Current	Photodetector Amplifier Gain	Light Output	Multiplication factor
Step-1	Normal Setting (I_{N1})	Fixed value (K_1)	L_1	L_1/L_2 (Current)
Step-2	Reduced Settings (I_{R1})	Fixed value (K_1)	L_2	
Step-3	Fixed value (K_2)	Normal Settings (G_{N1})	L_3	L_3/L_4
Step-4	Fixed value (K_2)	Reduced Settings (G_{R1})	L_4	(Gain)

photodetector amplifier gain setting is G_{R1} , then multiplication factors can be calculated using (7) and (8).

$$\text{Current Multiplication factor (CM)} = \frac{I_{N1}}{I_{R1}} \dots \quad (7)$$

$$\text{Gain Multiplication factor (CM)} = \frac{G_{N1}}{G_{R1}} \dots \quad (8)$$

Method-2: The LED current accuracy (current error) and photodetector amplifier gain accuracy (gain error) of AFE module for normal settings and reduced settings may be different. Manufacturing tolerance for current and gain is given in data sheets of AFE modules. Hence, estimation of incident intensity by simply considering predetermined gain and current multiplication factors, may not always be accurate. To address this issue we introduced a UV-NIR Neutral Density Filter (ND Filter). The device can measure the attenuated intensity value for a material with known attenuation thereby eliminating the possibility of saturation of the photodetector amplifier. A UV-NIR ND Filter from Edmund Optics with an optical density of 1.3 (5% light transmission) was used in our study. Fig. 8 shows a picture of the ND filter used.

The ND filter was positioned in the finger slot between the light source and the photodetector. The device was then made to run with four different current and gain settings sequentially as tabulated in Table IV. The ND filter attenuates 95% of light for each wavelength and 5% of the light is picked by the photodetector. The attenuated light outputs measured in the four steps (L_1 , L_2 , L_3 and L_4) are then used to determine the current and gain multiplication factors.

3) Hemoglobin Estimation: PPG data was collected using the proposed device architecture from 1005 women from India with the intention of (i) analyzing the signal quality of PPG data collected across a wide range of Hemoglobin (Hb) values from the device, and (ii) proving the efficacy of Hb estimation using this data. Details of this data collection

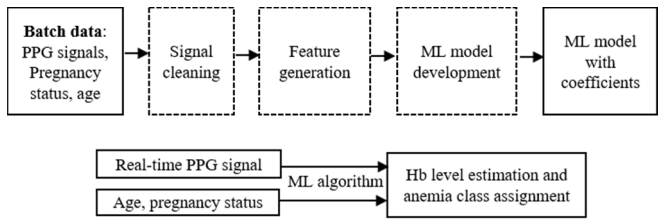


Fig. 9. Data processing and algorithm.

protocol are provided as part of another study [33]. The data collection procedure was conducted in collaboration with Department of Public Health at Manipal University, Karnataka and in compliance with medical ethics committee requirements (MUEC/012/2016-17).

The signal quality of the PPG signals was assessed by visual inspection. The Hb estimation was carried out by designing and training a machine learning algorithm. The PPG signals, once collected, were pre-processed to remove motion artefacts and other signal noises. A set of features were developed using the incident and attenuated light intensities. Four attenuated intensity values were calculated from the pulsatile components of four PPG waveforms corresponding to light from the four LEDs (590 nm, 660 nm, 810 nm and 940 nm). A total of eleven features were generated: four attenuation values; five ratio of ratios; age and pregnancy status [34]. The dataset was divided into 80% training set and 20% testing set and was used to train four regressor models: LASSO (Least Absolute Shrinkage and Selection Operator), Ridge Regression, Elastic Net Regression and Ada Boost. Predictions from these different regression models were fed into a Stacked Regressor Model [35], which provided the final prediction of Hb value (Fig. 9). This process was repeated 15 times, metrics were calculated in each iteration and averages were calculated. Performance of this machine learning model was evaluated with respect to the Hb values measured by standard automated cell counters using Root Mean Square Error (RMSE), correlation between the true and predicted Hb values and the goodness of fit plot. The details of the prediction algorithm are provided as part of another study [34].

III. RESULTS AND DISCUSSION

A. Single Point Light Source

Fig. 10 shows the intensity distribution profile and Table V summarizes the observations of each of the seven combinations of LED and the optical coupling assemblies, as tabulated in Table II. A non-uniform intensity distribution profile was observed for the four LEDs in the combinations of CPC with wide emission SMD LED (combination-2), narrow emission through hole LED (combination-5) and Multiwavelength LED without any coupling (combination-7). Their maximum offset from the center was high and hence these combinations were deemed un-suitable to form a single-point light source for the current study. Although, it was observed that the combination of CPC with narrow emission LED assembly has better intensity distribution than that of CPC with wide emission LED assembly.

Out of combinations 1, 3, 4 and 6, high transmission losses were observed for the combinations 3 and 6 and were

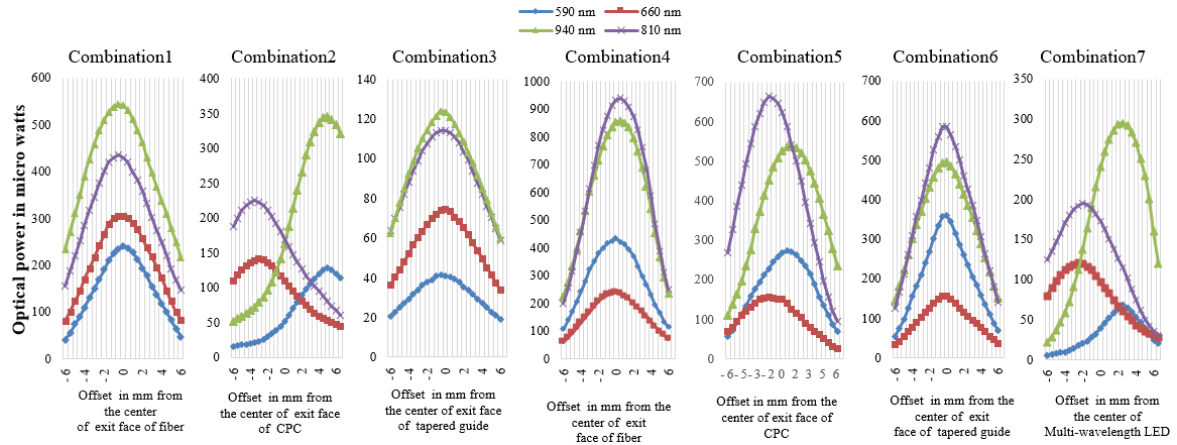


Fig. 10. The light intensity distribution LED with coupling optics for combination 1-7.

TABLE V
TEST RESULTS FOR THE SEVEN COMBINATIONS

Options	Maximum offset from center	Coupling & transmission loss	Ease of mechanical integration
Combination1	Less	Less	Easy
Combination2	Very high	High	Easy
Combination3	Less	Very high	Fragile
Combination4	Very low	Less	Easy
Combination5	Low	High	Easy
Combination6	Very low	Very high	Fragile
Combination7	Large	Less	Easy

TABLE VI
TEST RESULTS FOR REPEATED TRIALS FOR COMBINATION4

No. of Trials	Maximum (peak) optical power level available at the photodetector in milli Watts				Offsets of peak optical power from the center of the light guide in milli metre			
	590nm	660nm	810nm	940nm	590nm	660nm	810nm	940nm
T1	440	250	948	856	0.5	0	0	-1
T2	437	251	947	857	1	0	0	-0.5
T3	439	248	940	866	0.5	1	-1	0
T4	441	250	945	863	0	0	-0.5	-0.5
T5	442	248	940	866	0	1	-1	0
T6	437	249	942	855	1	1	-0.5	-1
T7	442	251	941	865	0	0	-1	0
T8	439	249	951	860	0.5	0.5	0	-0.5
T9	438	249	950	864	0.5	0.5	0	0
T10	440	250	940	856	0.5	0	-0.5	-1

hence opted-out. Out of combinations 1 and 4, we chose the combination of narrow band emission through hole LEDs and the optical fiber (Combination-4) to create a point-light source in this study. This was because the peak intensity of each wavelength was centered in alignment with the center of optical fiber and the amplitude of intensity was high. Integrating the tapered guide with LEDs was not easy, since they were long and easily breakable. Furthermore, the cost of optical fiber was much lesser than the cost of CPC and tapered guide.

Once Combination4 was chosen for the proposed device architecture, repeated trials (Table VI) were implemented and the maximum intensity and its offset from the center of the light guide for all wavelengths were recorded. Deviation (error) of peak intensity was observed to be within $\pm 1\%$ and Maximum Offset of peak intensity of each wavelength was 1 mm. Intensity distribution profiles of point light source

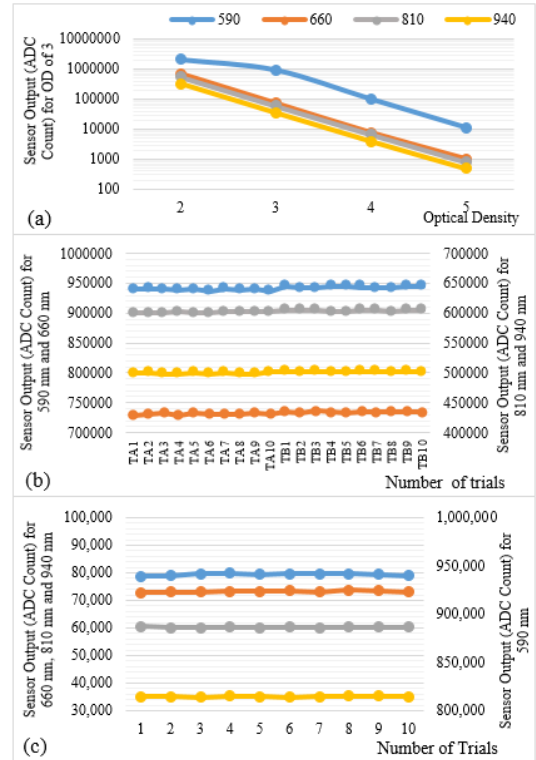


Fig. 11. (a) Sensor output vs optical density, (b) Sensor output for reduced light intensity vs Number of trials with normal ambient light (TA) and bright light (TB), (c) Sensor output vs Number of trials for OD = 3.

TABLE VII
CURRENT AND GAIN SETTINGS FOR METHOD-2 FOR WAVELENGTH 660nm. VALUES HIGHLIGHTED IN GREEN AND ORANGE COLOR ARE COMMON FOR NORMAL AND REDUCED SETTINGS RESPECTIVELY FOR BOTH METHODS

Current and Gain settings for Method-2 (660nm)						
I _N	I _R	G _N	G _R	K ₁	K ₂	ADC count
14mA				100K		L ₁
	3.5mA			100K		L ₂
		250K			8ma	L ₃
			10K		8ma	L ₄

was accurate by ± 1 mm with respect to offset from the center of the light guide.

TABLE VIII
INCIDENT INTENSITIES MEASURED BY METHOD-1 AND METHOD-2

Device No.	Reduced Intensity	Method-1		Method-2						Current error % = $[(M_{12}-M_{11})/M_{12}]*100$	Gain error % = $[(G_{12}-G_{11})/G_{12}]*100$	% deviation of Method-1 w.r.t Method-2
		$M_{11}=I_N/I_R=4$	$M_{G1}=G_N/G_R=25$	L_1 (ADC count)	L_2 (ADC count)	L_3 (ADC count)	L_4 (ADC count)	CM	$M_{G2}=L_3/L_4$	Actual Incident Intensity		
1	896999	743507278	628749	159180	928997	34176	3.95	27.71	98180577	-1.266	9.78	8.64
2	931908	536136162	544351	137872	808087	29755	3.95	27.42	100934024	-1.266	8.826	7.67
3	898989	616077663	584478	149695	872481	31632	3.9	27.44	96206207	-2.564	8.892	6.56
4	935998	840771254	560675	141600	833130	30292	3.96	26.92	99780382	-1.01	7.132	6.19
5	1005075	464084871	574944	145643	851489	31346	3.95	26.98	107111848	-1.266	7.339	6.17
6	876620	686201043	570216	143564	846124	30767	3.97	27.75	96575034	-0.756	9.91	9.23

Sensitivity of the device, which was defined as the minimum amount of transmitted intensity detected by the photodetector, was checked by introducing light absorbing elements (ND filters) with known optical density in the finger slot. The device was operated with the same LED intensity and photodetector gain settings as used for PPG capturing for all wavelengths. **Figure 11(a)** shows the ADC output of amplified photodetector signal versus optical density. Maximum count of the inbuilt ADC in the AFE module was 2097151. ADC output reached saturation for an OD of 2 for 590 nm due to its higher intensity. OD of the finger is >3 for all 4 wavelengths. The device could detect the light signals with an OD as high as 5 (99.999% light absorption) implying its sensitivity to be 0.001% of the incident light intensity.

The device was also tested for repeated trials for a fixed OD (**Fig. 11(b)**). Maximum deviation for all four wavelengths was observed to be within 1%. Same experiment was also repeated under bright light, but owing to the closed type probe design which prevents ambient light from entering the photodetector sensor, this did not impact the measurements (**Fig. 11(c)**). In all, the device showed a stable performance.

Proper arrangement of the point light source (no axial or lateral offset between optical fiber inside the top optical assembly), stable mechanical assembly, proper placement of the finger within the finger slot and no motion artefacts ensured a stable and repeatable performance of the device.

B. Incident Intensity

Incident intensities were calculated using Method-1 and Method-2 for six prototypes of the proposed device architecture. **Table VII** provides the current and gain setting values for the wavelength 660 nm for these six devices. **Table VIII** provides the calculation of the incident intensity values from these two methods. The values L_1 to L_4 are provided in units of ADC counts. Deviation in the estimation of incident intensity as calculated by Method-1 with respect to that of Method-2 is provided. The current and gain errors of AFE modules have also been tabulated.

Since the ND filter technique (Method-2) measures the intensity of light with normal and reduced settings directly to calculate the multiplication factors, it can be considered to be relatively more accurate than the Method-1. This analysis demonstrates the errors in the measurement without any consideration to device to device variation of the AFE modules. These errors are bound to be reflected in the estimation of incident intensity if the predetermined current and gain

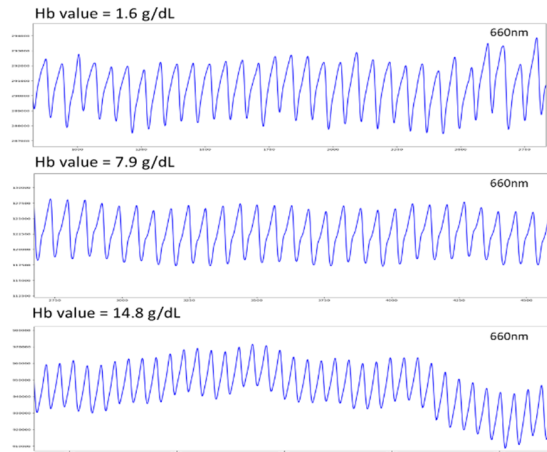


Fig. 12. PPG signal as captured by the proposed device for three Hb values.

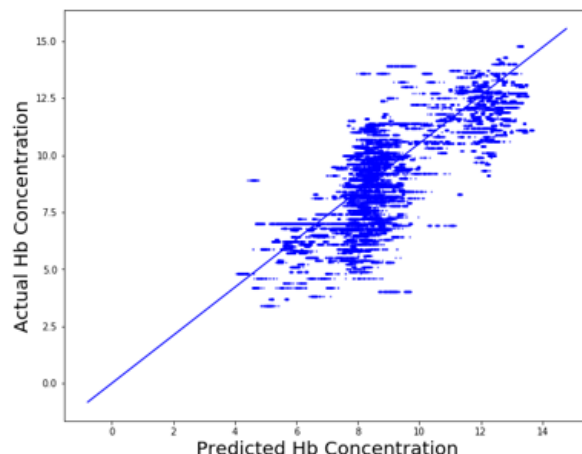


Fig. 13. Goodness of fit plot between predicted and actual Hb values.

multiplication gain were employed in the computation without using the ND filter technique.

C. Signal Quality and Hemoglobin Estimation

The device architecture was able to capture clear and noise free PPG signals for subjects having hemoglobin concentrations as low as 1.6 g/dL. **Figure 12** shows the raw PPG signals for three such Hb values as captured by the device. As can be observed, the signal quality is consistently good, thereby validating the use of this device across the Hb spectrum.

The Hb values predicted by the algorithm were compared with standard invasive method based automated cell counters. The performance of the Stacked Regressor model gave a root mean squared error (RMSE) of 1.47 ± 0.08 g/dL and a correlation of 0.79 ± 0.03 between the predicted and actual value of Hb. Fig. 13 depicts the graph plotting the actual vs predicted Hb values.

IV. CONCLUSION

In this study, we propose a novel device architecture for capturing multiwavelength PPG signals and estimating blood hemoglobin values of an individual. The device architecture consists of a single-point light source (for the multiple wavelengths) made of narrow band emission through hole LEDs coupled to an optical fiber light guide, a finger slot, a photodetector, an AFE board and an SBC.

The architecture is designed such that the point light source, the finger slot and the photodetector are always in a straight line for all finger sizes. This alleviates the problems of multiple path lengths, optical bypassing and misalignment. The device also measures the incident intensity each time it is powered-on in order to avoid the effects of degradation of LED intensity over time on the measurements. It makes use of the device-specific multiplication factors pre-determined using ND filters and stored in the memory of the device. The information extracted from the PPG signals thus captured by the device can be used to derive at an estimation of blood hemoglobin value using a built-in algorithm.

Currently anemia screening is done via expensive and/or invasive techniques requiring trained technicians and laboratory facilities. Device based on such techniques are not accessible to a large part of the rural population where the prevalence of anemia is high. The proposed device architecture, along with the built-in algorithm to estimate hemoglobin is portable, quick, battery-operated, easy-to-use and can estimate the hemoglobin values with reasonable accuracy without the need of hi-tech laboratories.

A few noninvasive devices are currently available for anemia screening, but they are expensive and lack reliability in detecting extremely low Hb levels, probably owing to poor-signal quality at low hemoglobin values or lack of data in this range for training the algorithms. The proposed device architecture could provide us good PPG signal quality at Hb values as low as 1.6g/dL. Also, a recent review [29], done on the commercially available noninvasive devices show that, the results were prone to ambient light. The closed type linear probe presented in this study prevents the entry of ambient light to the measurement site thereby providing better robustness to ambient light. With improved training dataset in the low hemoglobin value range, the clinical applicability of the proposed device can be further enhanced.

The proposed device is also intended to be a low-cost device. The components of the device include inexpensive parts like through hole LEDs, polymer optical fiber and silicon photo diode. Based on the hardware used for the current study, the cost of manufacturing one device may approximate to 70 USD (30 USD for SBC, 30 USD for AFE/LED boards and 10 USD for optics/mechanical assemblies) for a volume

of 10,000 devices. These costs are significantly lower than the cost of the commercially available noninvasive devices (Table-I).

Further enhancements in the device like IoT connectivity could equip the device with real-time monitoring and anemia screening by the community health workers (Asha workers). This could also assist in creating regional heat maps of anemia and strategize/formulate better health and anemia eradication programs in the country. Authorized cloud interface could enable remote access to results for in-depth investigations and regular follow-ups.

Leveraging the device architecture model proposed in this study, future studies can also be extended to measure other bio-analytes in the blood like glucose [32], creatinine [36] etc. This, equipped with recent advancements in the bio-sensing technology could aid in the non-invasive monitoring of many vital bio-analytes.

ACKNOWLEDGMENT

The authors would like to thank the Indian Institute of Science, Bangalore for their support during the course of the study. They would also like to thank the sensor design and methodology elaborated in this study are protected by several intellectual property (patents applications) held by Robert Bosch Engineering and Business Solutions Pvt Ltd.

REFERENCES

- [1] J. L. A. Nirupa and V. J. Kumar, "Non-invasive measurement of hemoglobin content in blood," in *Proc. IEEE Int. Symp. Med. Meas. Appl. (MeMeA)*, Lisboa, Portugal, Jun. 2014, pp. 1–5.
- [2] S. Chugh and J. Kaur, "Non-invasive hemoglobin monitoring device," in *Proc. Int. Conf. Control Commun. Comput. India (ICCC)*, Kerala, India, Nov. 2015, pp. 380–383.
- [3] R. A. Rochmanto, H. Zakaria, R. D. Alviana, and N. Shahib, "Non-invasive hemoglobin measurement for anemia diagnosis," in *Proc. 4th Int. Conf. Electr. Eng., Comput. Sci. Informat. (EECSI)*, Yogyakarta, Indonesia, Sep. 2017.
- [4] U. Timm, G. Leen, E. Lewis, D. McGrath, J. Kraitl, and H. Ewald, "Non-invasive optical real-time measurement of total hemoglobin content," *Procedia Eng.*, vol. 5, pp. 488–491, Sep. 2010.
- [5] U. Timm, E. Lewis, D. McGrath, J. Kraitl, and H. Ewald, "LED based sensor system for non-invasive measurement of the hemoglobin concentration in human blood," in *Proc. 13th Int. Conf. Biomed. Eng.*, Singapore, 2009, pp. 825–828.
- [6] U. Timm, E. Lewis, G. Leen, D. McGrath, J. Kraitl, and H. Ewald, "Non-invasive continuous online hemoglobin monitoring system," in *Proc. IEEE Sensors Appl. Symp. (SAS)*, Limerick, Ireland, Feb. 2010.
- [7] U. Timm, D. McGrath, E. Lewis, J. Kraitl, and H. Ewald, "Sensor system for non-invasive optical hemoglobin determination," in *Proc. IEEE Sensors*, Oct. 2009, pp. 1975–1978.
- [8] J. Kraitl, U. Timm, H. Ewald, and E. Lewis, "Non-invasive sensor for an *in vivo* hemoglobin measurement," in *Proc. IEEE SENSORS*, Limerick, Ireland, Oct. 2011, pp. 276–279.
- [9] K. J. Jeon, S. J. Kim, K.-K. Park, J.-W. Kim, and G. Yoon, "Noninvasive total hemoglobin measurement," *J. Biomed. Opt.*, vol. 7, pp. 45–50, Jan. 2002.
- [10] X. Yi, G. Li, and L. Lin, "Noninvasive hemoglobin measurement using dynamic spectrum," *Rev. Sci. Instrum.*, vol. 88, no. 8, Aug. 2017, Art. no. 083109.
- [11] C. Pinto, J. Parab, and G. Naik, "Non-invasive hemoglobin measurement using embedded platform," *Sens. Bio-Sens. Res.*, vol. 29, Aug. 2020, Art. no. 100370.
- [12] H. Liu *et al.*, "Development and validation of a photoplethysmography system for noninvasive monitoring of hemoglobin concentration," *J. Electr. Comput. Eng.*, vol. 2020, pp. 1–9, Jan. 2020.
- [13] M. Nitzan *et al.*, "Calibration-free pulse oximetry based on two wavelengths in the infrared—A preliminary study," *Sensors*, vol. 14, no. 4, pp. 7420–7434, Apr. 2014.

- [14] N. I. Khan, S. H. Choudhury, and A. A. Roni, "A comparative study of the temperature dependence of lasing wavelength of conventional edge emitting stripe laser and vertical cavity surface emitting laser," in *Proc. Int. Conf. Opt. Commun. Syst.*, Seville, Spain, 2011, pp. 18–21.
- [15] M. H. Mozaffari and A. Farmani, "On-chip single-mode optofluidic microresonator dye laser sensor," *IEEE Sensors J.*, vol. 20, no. 7, pp. 3556–3563, Apr. 2020.
- [16] N. Amoosoltani, N. Yasrebi, A. Farmani, and A. Zarifkar, "A plasmonic nano-biosensor based on two consecutive disk resonators and unidirectional reflectionless propagation effect," *IEEE Sensors J.*, vol. 20, no. 16, pp. 9097–9104, Aug. 2020.
- [17] M. A. Baqir, A. Farmani, T. Fatima, M. R. Raza, S. F. Shaukat, and A. Mir, "Nanoscale, tunable, and highly sensitive biosensor utilizing hyperbolic metamaterials in the near-infrared range," *Appl. Opt.*, vol. 57, no. 31, p. 9447, 2018.
- [18] E. Khosravian, H. R. Mashayekhi, and A. Farmani, "Tunable plasmonics photodetector in near-infrared wavelengths using graphene chemical doping method," *AEU, Int. J. Electron. Commun.*, vol. 127, Dec. 2020, Art. no. 153472.
- [19] H. Farmani and A. Farmani, "Graphene sensing nanostructure for exact graphene layers identification at terahertz frequency," *Phys. E, Low-Dimensional Syst. Nanostruct.*, vol. 124, Oct. 2020, Art. no. 114375.
- [20] E. J. Wang, W. Li, D. Hawkins, T. Gernsheimer, C. Norby-Slycord, and S. N. Patel, "HemaApp: Noninvasive blood screening of hemoglobin using smartphone cameras," in *Proc. UBICOMP*, Heidelberg, Germany, Sep. 2016, pp. 593–604.
- [21] E. Gayat, J. Aulagnier, E. Matthieu, M. Boisson, and M. Fischler, "Non-invasive measurement of hemoglobin: Assessment of two different point-of-care technologies," *PLoS ONE*, vol. 7, no. 1, Jan. 2012, Art. no. e30065.
- [22] F. Dietzel, P. Dieterich, F. Dörries, H. Gehring, and P. Wegerich, "Invasive and non-invasive point-of-care testing and point-of-care monitoring of the hemoglobin concentration in human blood—How accurate are the data?" *Biomed. Eng./Biomedizinische Technik*, vol. 64, no. 5, pp. 495–506, Sep. 2019.
- [23] N. Shah, E. A. Osea, and G. J. Martinez, "Accuracy of noninvasive hemoglobin and invasive point-of-care hemoglobin testing compared with a laboratory analyzer," *Int. J. Lab. Hematol.*, vol. 36, no. 1, pp. 56–61, Feb. 2014.
- [24] S. J. Barker, A. Shander, and M. A. Ramsay, "Continuous noninvasive hemoglobin monitoring: A measured response to a critical review," *Anesthesia Analgesia*, vol. 122, no. 2, pp. 565–572, Feb. 2016.
- [25] T. E. Morey, N. Gravenstein, and M. J. Rice, "Let's think clinically instead of mathematically about device accuracy," *Anesthesia Analgesia*, vol. 113, no. 1, pp. 89–91, Jul. 2011.
- [26] O. Wiebe, "Light absorbance in pulse oximetry," in *Design of Pulse Oximeters*. Bristol, U.K.: IOP Publishing, 1997, ch. 4, sec. 3.5.2, pp. 59–60.
- [27] M. V. S. Reddy, "Probes," in *Design of Pulse Oximeters*. Bristol, U.K.: IOP Publishing, 1997, ch. 7, sec. 11.5, pp. 108–109.
- [28] S. Tungjitsukulmorn, "Accuracy and errors," in *Design of Pulse Oximeters*. Bristol, U.K.: IOP Publishing, 1997, ch. 11, sec. 11.5, pp. 198–199.
- [29] S. Ardin, M. Störmer, S. Radojska, L. Oustianskaia, M. Hahn, and B. S. Gathof, "Comparison of three noninvasive methods for hemoglobin screening of blood donors," *Transfusion*, vol. 55, no. 2, pp. 379–387, Feb. 2015.
- [30] Y. Takamura, N. Kobayashi, S. Takeda, and T. Usuda, "Apparatus for measuring concentration of light-absorbing substance in blood," U.S. Patent 20040176670 AI, Sep. 9, 2004.
- [31] K. Urpalainen, "Development of a fractional multiwavelength pulse oximetry algorithm," M.S. thesis, School Electr. Eng., Aalto Univ., Espoo, Finland, 2011.
- [32] H. Ali, F. Bensaali, and F. Jaber, "Novel approach to non-invasive blood glucose monitoring based on transmittance and refraction of visible laser light," *IEEE Access*, vol. 5, pp. 9163–9174, May 2017.
- [33] S. Tungjitsukulmorn, "Accuracy and errors," in *Design of Pulse Oximeters*. Bristol, U.K.: IOP Publishing, 1997, ch. 11, sec. 11.2.3, pp. 195–196.
- [34] S. Acharya *et al.*, "Non-invasive estimation of hemoglobin using a multi-model stacking regressor," *IEEE J. Biomed. Health Informat.*, vol. 24, no. 6, pp. 1717–1726, Jun. 2020.
- [35] L. Breiman, "Stacked regressions," *Mach. Learn.*, vol. 24, no. 1, pp. 49–64, Jul. 1996.
- [36] A. H. Aly, D. Mohamed, M. A. Mohaseb, N. S. A. El-Gawaad, and Y. Trabelsi, "Biophotonic sensor for the detection of creatinine concentration in blood serum based on 1D photonic crystal," *RSC Adv.*, vol. 10, no. 53, pp. 31765–31772, 2020.



R. Dinesh Kumar received the bachelor's degree in electronics and communication, the Diploma degree in medical instrumentation, the M.Tech. degree in optoelectronics and laser technology from the International School of Photonics, Cochin University of Science and Technology, Kochi, India, and the Ph.D. degree in instrumentation from the Cochin University of Science and Technology.

He has been working with the Research and Development Centre of SFO Technologies from 2002 to 2013. He is currently working as a Senior Design Architect with Robert Bosch Engineering and Business Solutions, Bengaluru, India. He has ten international journal publications and also holds more than ten patents. His research interests include fiber optics, optoelectronics, lasers, analog, and RF systems.



S. Guruprasad received the bachelor's degree in engineering. He is also an Alumnus of the Indian Institute of Management, Bengaluru (IIMB). He is currently the Vice President with Robert Bosch Engineering and Business Solutions (RBEI). He directs business practices in emerging technologies of IoT, data sciences, and engineering in addition to domain vertical of health care. He is also one of the Directors with Bosch Healthcare Solutions, Germany, focusing on the portfolio of medical screening and software solutions worldwide.

He has been instrumental in furthering thought leadership and represents Robert Bosch as a member of various global forums and alliances. He has been associated with the Bosch Group since 2000. With two and a half decades of professional experience spanning diverse areas of engineering, information science, and corporate functions like business development, sales, and marketing, he has been instrumental in driving several innovation-led intrapreneurial businesses.



Krity Kansara received the master's degree in biomedical engineering from the Vellore Institute of Technology. She works as a Senior Engineer with Robert Bosch Engineering and Business Solutions Pvt. Ltd., Bengaluru, where she is responsible for bio-signal processing, algorithm development, and statistical data analyses as part of noninvasive healthcare product development. She has previously worked as a Senior Research and Development Engineer with the National Brain Research Centre, Gurgaon, and

other prestigious institutes like INMAS-Defense Research and Development Organization (DRDO) and the Indian Institute of Technology, Delhi (IITD), as part of multiple projects and internships in the fields of neuroscience and brain-computer interfaces. Her research interests include biomedical signal processing applied to healthcare engineering and neuroscience fields.



K. N. Raghavendra Rao was born in Bengaluru, India, in 1981. He received the B.E. degree in electronics and communication engineering from the M. S. Ramaiah Institute of Technology, affiliated to Visvesvaraya Technological University (VTU), a Collegiate Public State University, Belgaum, India, in 2003.

From 2004 to 2007, he was a Research and Development Engineer with the Healthcare Business Group, British Physical Laboratories. From 2008 to 2016, he was a Senior Technical Specialist with Philips Healthcare. Since 2016, he has been a Technical Architect with Robert Bosch Engineering and Business Solutions, Bengaluru, with the Engineering Healthcare Department, developing noninvasive, point of care health monitoring devices. His interests include biomedical signal processing and machine learning applications.



Murali Mohan was born in Tumkur, India, in 1985. He received the B.E. degree in instrumentation and electronics engineering from Visvesvaraya Technological University, Belgaum, India, in 2002, and the M.S. degree in automotive embedded systems from Manipal University, in 2011. He is also an Alumnus of the Indian Institute of Management, Bangalore (IIMB).

He has 14 years of professional experience, majorly in engineering and project management areas. He joined Robert Bosch Engineering and Business Solutions Pvt. Ltd., in 2012. He was a Software Developer for advanced driver assistance systems. He is currently the Product Manager in Healthcare Domain, responsible for the product engineering of medical devices. His research interest includes the development of AI/ML-based noninvasive screening medical devices.



P. Prakash was born in Kangeyam, Tiruppur, India, in 1981. He received the bachelor's degree in mechanical engineering from Bharathiar University, Coimbatore, India, in 2002, and the Post-Graduate Diploma degree in plastics engineering from CIPET, Chennai, India, in 2004.

He was a Mold Design Engineer of Plastics Components Used in Electronics Products from 2004 to 2010 with Laxmi Electronics Bengaluru. Since 2010, he has been working with Robert Bosch Engineering and Business Solutions Pvt. Ltd., India, as a Design Engineer in the design and development of power tools and medical products. He is currently working as an Architect of New Product Development for Mechanical Design with Robert Bosch (RBEI).



Manjunath Ramakrishna Reddy received the bachelor's degree in electronics and communication from Bangalore University in 2001.

He works as the Technical Project Manager with Robert Bosch Engineering and Business Solutions Pvt. Ltd., Bengaluru. He is with Bosch for more than 15 years in various roles for developing embedded solutions across different domains in security systems, industrial automation, thermo technology, healthcare, and mobility solutions. Previous to Bosch, he has worked with

Bharath Electronics Ltd., close to two years on manufacturing and test software development for defense equipment.



Uday Haleangadi Prabhu received the bachelor's degree in instrumentation technology from Bangalore University in 1992.

He is the Head of Innovation, Connected IoT Products and Digital Labs with Robert Bosch Engineering and Business Solutions Pvt. Ltd., Bengaluru, India. He has been in the industry for 28 years in new products innovation covering the geographies of India, the U.K., Germany, the USA, and Australia. He has been with Bosch for more than 14 years in various roles and

market segments and has been involved in automotive, consumer, industrial, and energy business units within Bosch. His current research interests include developing innovative edge solutions in the space of industry, mobility, consumer, energy, healthcare, and transport with a horizontal focus in the areas of smart AI/ML-based product design, connected devices, smart sensing, business model innovation, and product research and development. He has a past industry experience of around ten years with Infosys in the engineering services space, five years of running a startup developing new products for the industrial and robotic equipment markets, and managing large programs. His experience has spanned multiple disciplines with a high focus on systems engineering and design.



Sushovan Chakraborty received the master's degree in applied statistics and informatics from the Indian Institute of Technology Bombay (IIT-B). He is associated with Robert Bosch Engineering and Business Solutions Pvt. Ltd., (RBEI), Bengaluru, a fully owned subsidiary of Robert Bosch GmbH, Germany, as a Data Scientist for the last six years. He has been instrumental in conceptualizing and developing multiple solutions centered on artificial intelligence (AI) for

healthcare and was involved in co-authoring publications on similar topics. Some of the publications he coauthored are noninvasive estimation of hemoglobin using a multimodel stacking regressor and a scalable and reactive big data architecture design for predictive maintenance of connected cars.



Sreetama Das received the B.Sc. and M.Sc. degrees in physics from Jadavpur University, Kolkata, and the Ph.D. degree in biophysics and computational biology from the Indian Institute of Science, Bengaluru. She has been a Senior Data Scientist with Robert Bosch Engineering and Business Solutions Pvt. Ltd., Bengaluru, since 2017, where she is responsible for solution design and algorithm development across different industry verticals. She has worked on multiple projects in health care and manufacturing sectors

using machine learning and computer vision. Her research interests include the application of machine learning to molecular life sciences and healthcare data, with several research publications on those topics.



K. N. Madhusoodanan received the M.Sc. and Ph.D. degrees in physics from the Cochin University of Science and Technology, Kochi, India, in 1983 and 1989, respectively.

He carried out Postdoctoral Research work with the Indian Institute of Science, Bangalore, India, II University Roma, Rome, Italy, Katholic University, Leuven, Belgium, and the Research Center Rossendorf, Dresden, Germany. He is currently the Vice-Chancellor and a Professor of Instrumentation with the Cochin University of Science and Technology. He has published over 120 research articles on topics, such as photoacoustic and photothermal techniques, amorphous semiconductors, ion-implanted Si and SiC, CVD diamond, fiber optic sensors, and gas sensors. His current research interest includes sensor materials and devices, soft computing methods for instrumentation, optical fiber sensors, the Internet of Things (IoT), and communication, and healthcare.